Winter 1-1-2010

On the Origin of the Highest Redshift Gamma-Ray Bursts

Krzysztof Belczynski
Los Alamos National Laboratory & Astronomical Observatory, University of Warsaw &

Daniel E. Holz
Los Alamos National Laboratory

Chris L. Fryer
Los Alamos National Laboratory

Edo Berger
Harvard-Smithsonian Center for Astrophysics

Dieter H. Hartmann
Department of Physics and Astronomy, Clemson University, hdieter@clemson.edu

See next page for additional authors

Authors

Krzysztof Belczynski, Daniel E. Holz, Chris L. Fryer, Edo Berger, Dieter H. Hartmann, and Brain O'Shea

ON THE ORIGIN OF THE HIGHEST REDSHIFT GAMMA-RAY BURSTS

KRZYSZTOF BELCZYNSKI[1,2,6], DANIEL E. HOLZ[1], CHRIS L. FRYER[1], EDO BERGER[3], DIETER H. HARTMANN[4], AND BRIAN O'SHEA[5]

[1] Los Alamos National Laboratory, Los Alamos, NM 87545, USA; kbelczyn@nmsu.edu, daniel@restmass.com, clfreyer@lanl.gov
[2] Astronomical Observatory, University of Warsaw, Al. Ujazdowskie 4, 00-478 Warsaw, Poland
[3] Harvard-Smithsonian Center for Astrophysics, 60 Garden St., Cambridge, MA 02138, USA; eberger@astro.princeton.edu
[4] Department of Physics and Astronomy, Clemson University, Clemson, SC 29634-0978, USA; hdieter@CLEMSON.EDU
[5] Department of Physics and Astronomy, Michigan State University, East Lansing MI 48824, USA; oshea@msu.edu

ABSTRACT

GRB 080913 and GRB 090423 are the most distant gamma-ray bursts (GRBs) known to date, with spectroscopically determined redshifts of $z = 6.7$ and $z = 8.1$, respectively. The detection of bursts at this early epoch of the universe significantly constrains the nature of GRBs and their progenitors. We perform population synthesis studies of the formation and evolution of early stars, and calculate the resulting formation rates of short- and long-duration GRBs at high redshift. The peak of the GRB rate from Population II stars occurs at $z \sim 7$ for a model with efficient/fast mixing of metals, while it is found at $z \sim 3$ for an inefficient/slow metallicity evolution model. We show that in the redshift range $6 \lesssim z \lesssim 10$, essentially all GRBs originate from Population II stars, regardless of the metallicity evolution model. These stars (having small, but non-zero metallicity) are the most likely progenitors for *both* long GRBs (collapsars) and short GRBs (neutron star–neutron star or blackhole–neutron star mergers) at this epoch. Although the predicted intrinsic rates of long and short GRBs are similar at these high redshifts, observational selection effects lead to higher (a factor of $\sim$10) observed rates for long GRBs. We conclude that the two recently observed high-z GRB events are most likely long GRBs originating from Population II collapsars.

Key words: binaries: general – gamma rays: bursts – stars: formation

Online-only material: color figures

1. INTRODUCTION

The *Swift* satellite has recently discovered two high-redshift gamma-ray bursts (GRBs): GRB 080913 at redshift $z = 6.7$ (Schady et al. 2008) and GRB 090423 at redshift $z = 8.1$–8.3 (Tanvir et al. 2009, Salvaterra et al. 2009). The gamma-ray properties of these bursts straddle the traditional dividing lines between short and long bursts, making a solid classification of each burst difficult. For example, the observed burst duration of GRB 080913, $\sim$8 s, classifies it as a long GRB (Stamatikos et al. 2008). However, in the rest frame of the burst the duration is $\sim$1 s, suggesting a short GRB (Perez-Ramirez et al. 2008). It has been argued that, despite its relatively short duration (in the comoving frame), GRB 080913 nonetheless should be classified as a long GRB due to the specifics of the category definition (which places the dividing line at 2 s in the observer frame, for a GRB sample with mostly unknown redshifts), and because other properties of this burst (e.g., the lag–luminosity and Amati 2006 relations) are consistent with those of long GRBs (Greiner et al. 2009). Similarly, GRB 090423 had a burst duration of $\sim$9 s and a rest-frame duration of $\sim$1 s. Although many of the gamma-ray diagnostics of this burst (T_{90}, E_{peak}, hardness ratio) would classify it as "short" had the burst occurred at low redshift, it has been argued that GRB 090423, as in the case of GRB 080913, is a "long" burst (Salvaterra et al. 2009; Zhang et al. 2009).

We employ two simplifications of nomenclature. First, we retain the use of the "short" and "long" classifications for GRBs, despite growing evidence that the classification should be determined using a broader set of criteria beyond merely burst duration (Donaghy et al. 2006; Zhang et al. 2007; Bloom et al. 2008). Second, we tie these two classifications to specific progenitors using the simple theory correspondences outlined in Popham et al. (1999). Long GRBs are believed to be associated with the deaths of massive stars and the associated formation of black holes (e.g., Woosley 1993; Galama et al. 1998; Hjorth et al. 2003; Stanek et al. 2003; Woosley & Bloom 2006). Short GRBs, on the other hand, are thought to originate from the merger of compact objects, such as double neutron star (NS–NS) or black hole–neutron star (BH–NS) binaries (e.g., Paczynski 1986; Eichler et al. 1989; Nakar 2007 and references therein). An alternative, unified model for GRBs has been proposed to simultaneously explain both long and short GRBs in terms of the same underlying physical mechanism, involving a black hole as central engine (e.g., Ruffini et al. 2006; Dar & Rujula 2004). In addition, there exist models for both short and long GRBs that do not involve black holes (e.g., Usov 1992; King et al. 2007; Cheng & Dai 1996). A preferable classification of bursts might focus on the progenitor classification of each bursts, which depends upon supernova (SN) association, host galaxy type, metallicity, and offset of the GRB with respect to the host galaxy (see Fryer et al. 2007 for a review). In this paper, we study the progenitors directly, and identify collapsars with long GRBs, and compact object mergers with short GRBs.

Given their cosmological nature, and their bright afterglows, GRBs are unique tools to probe cosmological parameters and the structure and composition of matter along the GRB sightlines (e.g., Lamb & Reichart 2000; Lloyd-Ronning et al. 2002; Gou et al. 2004; Prochaska et al., 2007; Lamb 2007; Hartmann 2008; Savaglio et al. 2009; Piro et al. 2009; Hartmann et al. 2009). This argument gains force with the discovery of GRBs at very high redshifts; for example, GRB 050904 at $z = 6.29$ (Cusumano et al. 2006; Kawai et al. 2006), and now GRB 080913 and GRB 090423 beyond the furthest quasars (e.g., CFHQS J2329−0301 at $z = 6.4$; Willot et al. 2007) and the furthest spectroscopically confirmed galaxies (galaxy IOK-1; J132359.8+272456, at $z = 6.96$; Iye et al. 2006). These high-redshift objects provide

---

[6] Oppenheimer Fellow.

a unique opportunity to study the universe during the extended, inhomogeneous epoch of reionization, tracing cosmic star formation back to the first generation of stars (Population III). GRB follow-up observations have the potential to reveal the fraction of neutral hydrogen and metal abundances as a function of redshift, possibly beyond $z \sim 10$, with future instrumentation on large aperture telescopes on the ground and in space. GRBs constrain star formation models in the pristine universe, and serve as unique light sources to pinpoint star formation activity even in the smallest protogalaxies which would otherwise remain undetected. Rapid absorption spectroscopy of their afterglows offers a truly exceptional opportunity for studies of cosmic chemical evolution in an otherwise inaccessible part of the cosmic baryon field. However, in order to utilize these distant GRBs as probes, prompt localization and redshift determination is crucial. Currently, the *Swift* satellite performs rapid response observations in the X-ray and optical–UV bands. Future missions, such as the Energetic X-ray Imaging Survey Telescope (EXIST; Grindlay 2006), will provide combined wide-field X-ray and near-infrared imaging spectroscopy to study distant GRBs and associated black hole formation in the early universe.

In this study, we attempt to characterize the progenitors of GRB 080913 and GRB 090423, and other potential GRBs at these high redshifts. As we shall see, this epoch is entirely dominated by Population II stars and we focus on GRBs produced only from these stars. We analyze the formation of stars at high redshift in Section 2. In Section 3, we use a self-consistent model to follow in detail the evolution of the most likely GRB progenitors: massive stars, and NS–NS/BH–NS mergers. In Section 4, we adopt a cosmological model to estimate the GRB intrinsic (Section 5) and observed (Section 6) event rates at high redshift, explicitly identifying the likely progenitors of GRB 080913 and 090423. We conclude in Section 7.

2. STELLAR POPULATIONS: MODEL/RESULTS

Star formation history. To derive rates for various stellar events (SNe, mergers, etc.) one must start from a star formation rate (SFR) history, and add assumptions about the cosmic evolution of basic properties such as the initial mass function (IMF) and the fraction of stars in binaries. We use the analytic cosmic SFR prescription provided by Strolger et al. (2004):

$$\mathrm{sfr}(t) = 10^9 a(t^b e^{-t/c} + d e^{d(t-t_0)/c}) \ M_\odot \ \mathrm{yr}^{-1} \ \mathrm{Gpc}^{-3}, \quad (1)$$

where t is the age of universe (in gigayears) as measured in the global comoving (rest) frame, t_0 is the present age of the universe ($t_0 = 13.47$ Gyr; see Section 4), and we adopt parameters corresponding to the extinction-corrected model: $a = 0.182$, $b = 1.26$, $c = 1.865$, $d = 0.071$. The SFR density described above is in comoving units (space as well as time); for a non-evolving population, this rate is constant.

Galaxy mass distribution. At redshift $z < 4$, we describe the distribution of galaxy masses using a Schechter-type probability density function (pdf), calibrated to observations from Fontana et al. (2006):

$$\Phi(M_{\mathrm{gal}}, z) = \Phi^*(z) \ln(10) a^{1+\alpha(z)} e^{-a}, \quad (2)$$

with $\Phi^* = 0.0035(1 + z)^{-2.20}$, $a = 10^{\log(M_{\mathrm{gal}}) - M_z}$, $M_z = 11.16 + 0.17z - 0.07z^2$, and $\alpha(z) = -1.18 - 0.082z$. A galaxy mass, M_{gal}, in units of $M_\odot$, is drawn from this distribution (Equation (2)) in the range $7 < \log(M_{\mathrm{gal}}) < 12$. For galaxies at

redshifts beyond $z = 4$ we use the above distribution evaluated at $z = 4$, i.e., we assume no evolution in the galaxy mass distribution at earlier times. This assumption reflects the lack of information on galaxy mass distributions at high redshift. Although this may be a decent approximation at intermediate redshifts ($4 \lesssim z \lesssim 10$), it is almost certainly incorrect at very high redshift, where only low-mass galaxies (and Population III stars) are forming.

Galaxy metallicity. We assume that the average oxygen to hydrogen number ratio (F_{OH}) of a typical galaxy depends on its mass as

$$\begin{aligned}
\log(F_{\mathrm{OH}}) &= \log(10^{12} \mathrm{O/H}) \\
&= sz + 1.847 \log(M_{\mathrm{gal}}) - 0.08026(\log(M_{\mathrm{gal}}))^2,
\end{aligned} \quad (3)$$

with a redshift-independent normalization $sz = -1.492$ (Tremonti et al. 2004). It has been suggested that the functional form of this mass–metallicity relation is redshift independent (Erb et al. 2006; Young & Fryer 2007), with only the normalization factor, sz, varying with redshift. We characterize the redshift dependence of galaxy metallicities using the average metallicity relation from Pei et al. (1999):

$$Z \propto \begin{cases} 10^{-a_2 z} & z < 3.2 \\ 10^{-b_1 - b_2 z} & 3.2 \leqslant z < 5 \\ 10^{-c_1 - c_2 z} & z \geqslant 5 \end{cases}, \quad (4)$$

which implies evolution of the normalizing factor, sz, with redshift given by

$$sz \propto \begin{cases} -a_2 z - 1.492 & z < 3.2 \\ -b_2 z - 3.2(a_2 - b_2) - 1.492 & 3.2 \leqslant z < 5 \\ -c_2 z - 5(b2 - c2) & \\ \quad -3.2(a2 - b2) - 1.492 & z \geqslant 5. \end{cases} \quad (5)$$

With this approach, we assume that the oxygen abundance (used in F_{OH}) correlates linearly with the average abundance of elements heavier than helium (which is what is provided in the metallicity measure, Z). The normalization given by Pei et al. (1999) is $a_2 = 0.5$, $b_1 = 0.8$, $b_2 = 0.25$, $c_1 = 0.2$, $c_2 = 0.4$. We also derive the coefficients from the metallicity dependence proposed by Young & Fryer (2007), based on ultraviolet (*Galaxy Evolution Explorer* (*GALEX*), Sloan Digital Sky Survey), infrared (*Spitzer*), and neutrino (Super-Kamiokande) observations (Hopkins & Beacom 2006): $a_2 = 0.12$, $b_1 = -0.704$, $b_2 = 0.34$, $c_1 = 0.0$, $c_2 = 0.1992$. The Pei et al. (1999) normalization results in a relatively slow metallicity evolution as compared with the model of Young & Fryer (2007), which allows for a rapid increase of the average metallicity of stars with time. This is shown in Figure 1 (top panel), which provides the metallicity distribution of stars. It is apparent that for the *fast* model the metallicity of stars is on average an order of magnitude higher than for the *slow* model at the same high ($z = 7$) redshift.

Using Equations (3) and (5), we estimate the average galaxy oxygen to hydrogen ratio, given the mass and redshift of a galaxy. We express our estimators relative to solar:

$$F_{\mathrm{OH,gal}} = F_{\mathrm{OH}}/F_{\mathrm{OH,\odot}}, \quad (6)$$

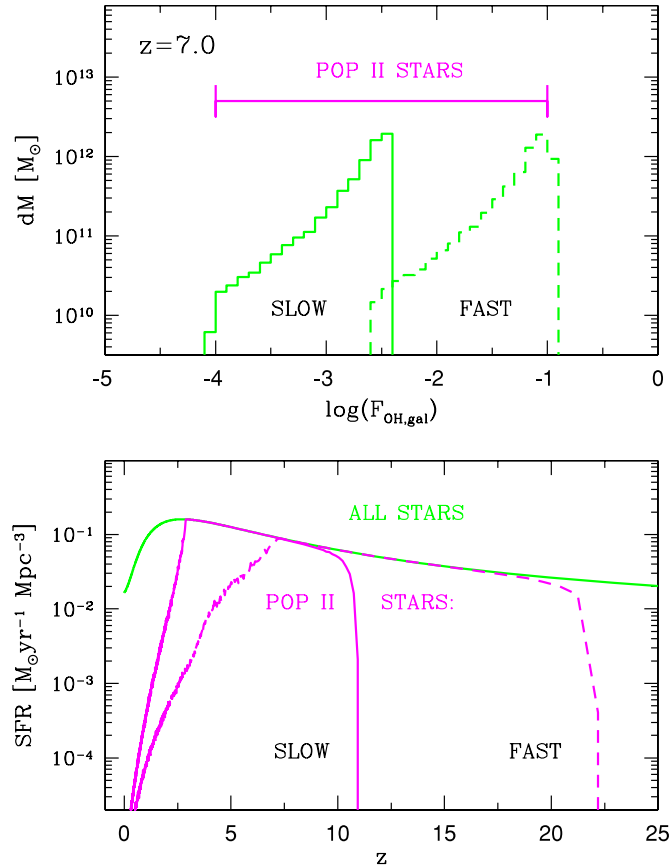where $F_{\mathrm{OH,\odot}} = 4.9 \times 10^8$ is the solar value (Tremonti et al. 2004).

Figure 1. Bottom panel: star formation rate history. We have adopted an extinction-corrected star formation rate model from Strolger et al. (2004): all stars. We also show the rate we have obtained for just Population II stars (see Section 2): the population is rather different for slow (solid) and fast (dashed line) metallicity evolution models. Top panel: metallicity distribution of stars at redshift $z = 7.0$. The results are shown for the two different adopted metallicity evolution histories: fast (Young & Fryer 2007) and slow (Pei et al. 1999). We mark our definition for Population II stars: it is clearly seen that independent of metallicity evolution majority of the stars belong to Population II at redshift that is typical for stars that may become (after appropriate delay) progenitors of GRB 080913.

(A color version of this figure is available in the online journal.)

Galaxy stellar population. We use the above galaxy metallicity estimator to formally delineate different stellar populations:

$$\begin{array}{ll} F_{\rm OH,gal} < 10^{-4} & \text{Population III} \\ 10^{-4} \leqslant F_{\rm OH,gal} \leqslant 10^{-1} & \text{Population II} \quad . \\ F_{\rm OH,gal} > 10^{-1} & \text{Population I} \end{array} \qquad (7)$$

Our choice for the lower metallicity bound (10^{-4}) on Population II marks the point where metals are abundant enough to provide sufficient cooling in the collapse of gas clouds, and thus star formation significantly deviates from the Population III stage (e.g., Mackey et al. 2003; Smith et al. 2009). It also marks the point where winds of massive stars are sufficiently strong to prevent the formation of pair-instability SNe (Heger et al. 2003). The choice for the Population II upper bound is dictated by the observation of Population I and II stars in the Milky Way (e.g., Binney & Merrifield 1998, Chapters 6 and 8; Beers & Christlieb 2005). Population I stars (e.g., disk and bulge stars) have metallicities that are approximately solar, with variations of a factor of 5. Population II stars (e.g., halo populations, such as stars in globular clusters) have metallicities at or below 10^{-1}–10^{-2} solar.

Each galaxy is assumed to host just one stellar population, determined by its metallicity. Since we draw a large number of galaxies at any given redshift (see Equation (2)) via Monte Carlo simulations, the use of an average metallicity measure is appropriate.

In Figure 1 (bottom panel), we show our assumed star formation history as a function of redshift, with the contribution from Population II stars highlighted. Population II stars form over a wide range of redshifts, starting at $z \sim 22$, and peaking at $z \sim 7$ for the fast metallicity evolution model. For the slow metallicity evolution, the interstellar medium is enhanced with metals much later, and Population II stars begin forming only at redshifts $z \sim 11$, peaking at $z \sim 3$. Although the metallicity evolution is poorly constrained, the two adopted models are most likely extremes, with the true evolution somewhere in between. For example, the transition from Population III to Population II stars is found to occur at $z \sim 11$ and $z \sim 22$ for our slow and fast metallicity evolution models, respectively. More sophisticated models place this limit at redshifts $z \sim 15$–20 (e.g., Mackey et al. 2003). Recent results show that Population III stars can form as recently as $z \sim 5$ (Schneider et al. 2006; Tornatore et al. 2007), but with rates significantly below that of Population II stars.

Population III stars were forming prior to the measured redshifts of GRB 080913 and 090423. Individual Population III stars may give rise to long GRBs in collapsar models with enhanced rotation (e.g., Yoon et al. 2006). However, as the lifetime of massive Population III stars is very short ($\sim$3–6 Myr; e.g., Schaerer 2002), these GRBs would be observed at much higher redshifts ($z \gtrsim 10$), tracing the Population III SFR with little delay. If binary Population III stars are formed, they could evolve into NS–NS/BH–NS systems that in turn, after an appropriate delay before merging, would give rise to short GRBs at potentially much lower redshift (however, see Ripamonti & Abel 2004 and O'Shea & Norman 2007, both of whom find that fragmentation does not occur in pristine clouds, implying that no Population III binaries would form). It has been argued that GRBs from such binaries, if they do form, would result in negligible detection rates for current detectors, including *Swift* (Belczynski et al. 2007).

The transition from Population II to Population I star formation begins at $z \sim 7$ for the fast or at $z \sim 3$ for the slow metallicity evolution model, continuing gradually until the present. Regardless of the metallicity evolution model, Population I stars are the dominant contribution to the SFR below $z \sim 2$, although a small number of Population II stars are also predicted at these lower redshifts. The earliest Population I stars begin forming at $z \sim 7$, but this is a negligible fraction of the total star formation at this redshift, even for the extreme fast metallicity evolution model (see Figure 1; top panel). Significant formation of Population I stars is found for redshifts $z \lesssim 6$ (fast) and $z \lesssim 2.5$ (slow), and thus Population I stars are unlikely to be the progenitors of high-z bursts.

Regardless of metallicity evolution models, Population II stars dominate the SFR at redshift $6 \lesssim z \lesssim 10$ (see Figure 1), and are the likely progenitors for both GRB 080913 and GRB 090423. Therefore, in the following we focus exclusively on Population II stars.

3. STELLAR EVOLUTION: MODEL/RESULTS

Evolutionary code. We use the `StarTrack` population synthesis code (Belczynski et al. 2002, 2008a), which employs the stellar evolution models of Hurley et al. (2000), to calculate

the population of low-metallicity stars, with $Z = 0.0001$ ($\sim 10^{-2.3} Z_\odot$). We evolve $N_{\rm bin} = 2 \times 10^6$ massive binary systems, with the mass of the primary (the initially more massive) member, M_1, drawn from a power-law IMF with the exponent -2.7 in the range 5–150 $M_\odot$. The secondary member's mass, M_2, is drawn randomly from a uniform initial mass ratio distribution ($q = M_2/M_1 \in 0 - 1$), where we only evolve binaries that have secondaries with $M_2 > 3 M_\odot$. Initial orbital separations, a, are drawn from a uniform random distribution in $\ln a$ (i.e., pdf $\propto 1/a$; Abt 1983), and eccentricities are taken from the distribution pdf $= 2e$ (e.g., Heggie 1975; Duquennoy & Mayor 1991).

We also evolve a population of $N_{\rm sin} = 2 \times 10^6$ massive single stars, with initial masses chosen as described above for the primary members of the binaries. The lower mass limits are chosen such that all stars that can potentially form either neutron stars or black holes are included in the calculations.

If the mass range is extended to the hydrogen-burning limit ($\sim 0.08 M_\odot$), one can estimate the total stellar mass that corresponds to our calculation (i.e., we evolve only the fraction of mass that is formed in massive stars, but for the purpose of rate calculations we also estimate the total stellar mass). We use a three-component power-law IMF; for stars with masses 0.08–0.5 $M_\odot$ the exponent is -1.3, for stars in the mass range 0.5–1 $M_\odot$ we use -2.2, and for masses above 1 $M_\odot$ we use -2.7 (Kroupa et al. 1993; Kroupa & Weidner 2003). Note that our population assumes an equal number of single and binary star systems, corresponding to a binary fraction $f_{\rm bi} = 50\%$ (or a binary system membership probability of 2/3 for any randomly selected star). Spectroscopic studies demonstrate that binary fractions are significant, especially for massive stellar populations (e.g., $\gtrsim 70\%$ for the Westerlund-1 cluster (Clark et al. 2008), or $\gtrsim 50\%$ for NGC6231 (Sana et al. 2008)). The total mass in our simulation, in single and binary stars over the entire mass range, is $M_{\rm sim} = 6.1 \times 10^8 M_\odot$.

Short GRBs. We extract from the population synthesis sample the NS–NS and BH–NS binaries with delay times shorter than 15 Gyr. The total number of short GRB progenitors is found to be $n_{\rm short} = 7.6 \times 10^3$ with 4.6×10^3 NS–NS and 3.0×10^3 BH–NS systems. The delay time, $t_{\rm del}$, is the time a given binary takes from the zero age main sequence to form a double compact object (evolutionary time, $t_{\rm evol}$) plus the time a double compact object takes to merge due to emission of gravitational radiation (merger time, $t_{\rm merger}$). The resulting delay time distribution is shown in Figure 2. The median delay time is 0.1 Gyr, with a mean of 1.5 Gyr and a standard deviation of 2.9 Gyr. In contrast to conventional wisdom, most mergers are expected shortly after the stars form, with only a small fraction (3.7%) of delay times in excess of 10 Gyr (qualitatively similar results for Population I stars were presented in Belczynski et al. 2006).

Long GRBs. We extract black holes (formed in both isolated stars and in binaries) that (1) formed through direct collapse (e.g., Fryer & Kalogera 2001) and (2) formed from a progenitor that at the time of core collapse was hydrogen depleted. The first condition ensures rapid accretion (~ 0.1–$1 M_\odot$ s^{-1}) onto a black hole. Popham et al. (1999) found that at least some of the power sources for GRBs are much more efficient at higher accretion rates, and Young & Fryer (2007) argue that current observations are better fit by these direct-collapse black holes. For the adopted Population II metallicity, single stars with initial mass $M_{\rm zams} > 23.8 M_\odot$ form black holes through direct collapse. Note that the limiting mass was 40.0 $M_\odot$ for solar metallicity, as obtained in Fryer & Kalogera (2001). Here
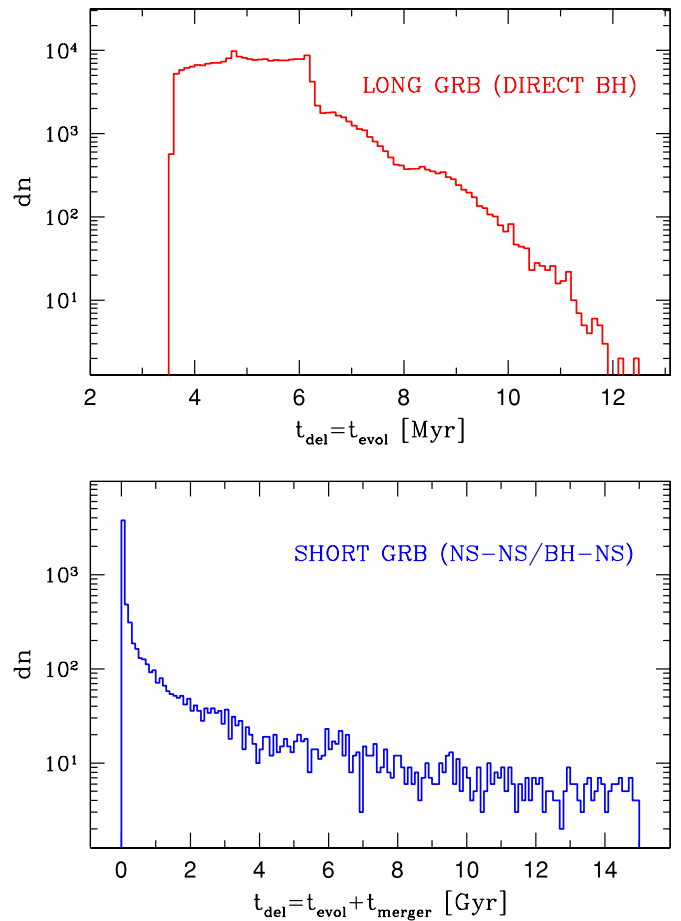

Figure 2. Top panel: delay times for long GRB progenitors: direct black holes that are formed out of H-depleted stars (both single and binary). Note the very short delay times of $\lesssim 6$ Myr. Delay is evolutionary time a star takes from the formation to a collapse. Bottom panel: delay times for short GRB progenitors: NS–NS and BH–NS mergers. Note that these events have significantly longer delay times than for the long GRB progenitors, with a median of 0.1 Gyr. Delay time is evolutionary time plus merger time.

(A color version of this figure is available in the online journal.)

we use different evolutionary models (Hurley et al. 2000), and we employ stellar winds that scale with metallicity as $\propto Z^{1/2}$, and find that stars with lower mass can potentially form black holes directly. However, we note that had we used 40.0 $M_\odot$ as a limiting mass for direct black hole (DBH) formation, our predicted rates for long GRBs would have remained virtually the same since condition (2) selects stars with mass that are above or close to the previous limit (see below). Our limit, which takes into account the effect of metallicity and stellar winds, is further modified by the presence of a binary companion (from rejuvenation and/or mass loss in close binaries).

The second condition allows for a GRB jet to punch through the outer layers of a star. A star may lose its H-rich envelope either through binary interactions or via stellar winds. Given the employed single star models, and the adopted metallicity, stars with $M_{\rm zams} > 35.9 M_\odot$ lose their entire H-rich envelopes via stellar winds. Binary interactions, on the other hand, may remove the envelope of a star of arbitrary mass. These conditions are insufficient to produce a GRB, since there must be just enough angular momentum in a collapsing star to form a lasting accretion torus (e.g., MacFadyen & Woosley 1999; Podsiadlowski et al. 2004). As angular momentum transport

is not taken into account in this study, our predictions only indicate potential long GRB progenitors, i.e., most likely only a (small) fraction of the events that satisfy (1) and (2) will actually produce long GRBs.

The total number of long GRB progenitors is found to be $n_{\text{long}} = 225 \times 10^3$ with 103×10^3 and 122×10^3 DBHs from H-depleted progenitors from single and binary stars, respectively. The delay time distribution is displayed in Figure 2. This represents the evolutionary time (t_{evol}) of a given star to form a black hole. The delay times for long GRB progenitors are very short, $\sim$3.5–12 Myr (as black holes form from massive and short-lived stars), with the median of the distribution at 5.1 Myr, a mean at 5.3 Myr, and a standard deviation of 1.1 Myr. These events thus trail the SFR, SFR(z), with very little delay, so that essentially one can assume that rate(DBH) $\propto$ SFR until very large redshifts.

4. COSMOLOGY: MODEL

We adopt a flat cosmology with $H_0 = 70.0$ km s^{-1} Mpc^{-1}, $\Omega_m = 0.3$, and $\Omega_\Lambda = 0.7$ (and thus $\Omega_k = 0$). Small ($\lesssim$10%) changes in the cosmological parameters leave our results essentially unaltered.

For clarity in what follows, we briefly review the relevant cosmological expressions. The relationship between redshift and time is given by

$$t(z) = t_{\text{H}} \int_z^\infty \frac{dz'}{(1+z')E(z')}, \qquad (8)$$

where $t_{\text{H}} = 1/H_0 = 14$ Gyr is the Hubble time (e.g., Hogg 2000), and $E(z) = \sqrt{\Omega_{\text{M}}(1+z)^3 + \Omega_k(1+z)^2 + \Omega_\Lambda}$. The resulting age of the universe is $t(0) = 13.47$ Gyr. It is to be noted that this is the rest-frame time, constituting what is measured by the wristwatches of local observers at any time and place in the universe, and thus is the appropriate quantity to use when discussing local physical processes. Observed event rates from sources distributed over cosmic time must be corrected for time dilation, $R(0) = R(z)/(1+z)$.

The comoving volume element, dV/dz, for a given solid angle, $d\Omega$, is given by

$$\frac{dV}{dz}(z) = \frac{c}{H_0} \frac{D_{\text{c}}^2}{E(z)} \, d\Omega, \qquad (9)$$

where c is the speed of light in vacuum, and where the comoving distance, D_{c}, is given by

$$D_{\text{c}}(z) = \frac{c}{H_0} \int_0^z \frac{dz'}{E(z')}. \qquad (10)$$

There are a number of steps necessary to calculate the expected GRB event rates. To summarize: for each bin in time, we estimate the total SFR. We then calculate the fraction of these stars which are Population II by incorporating the metallicity distribution of the galaxies at the given time. We then employ population synthesis results to determine the fraction of Population II stars that are progenitors of GRBs. With these results, we are able to apply the appropriate delay times and transform the progenitor formation rate in each bin in time to an actual GRB event rate, distributed over later times. We repeat this procedure over all bins in time, which results in a total GRB event rate as a function of time. We now go through each of these steps in detail.

We bin time over the range 0.13 Gyr $< t <$ 13.47 Gyr (0 $< z <$ 25), with a constant width of $dt = 10$ Myr. For each bin we obtain the SFR using Equation (1), evaluated at the center of the bin. We then generate a Monte Carlo sample of 10^4 galaxies in the bin, distributed according to Equation (2), with a total mass in galaxies given by $M_{\text{gal,tot}}$. For each galaxy, we estimate its average metallicity from Equation (3) and, based on our population criterion (Equation (7)), we determine the number of galaxies containing Population II stars. The total mass of galaxies with Population II stars is denoted $M_{\text{gal,II}}$. The fraction of mass that has formed Population II stars in a given bin is thus given by

$$F_{\text{pop,II}} = \frac{M_{\text{gal,II}}}{M_{\text{gal,tot}}}, \qquad (11)$$

since we have assumed that each galaxy hosts only one stellar population (determined by its average metallicity; see Section 2).

We measure rate densities in units of yr^{-1} Gpc^{-3}, in comoving units (time and space). In our scheme, a delay for a given event constitutes a shift in time of the relevant fraction of the rate density (see Equation (12)). The population synthesis results yield a list of Population II GRB progenitors, and their corresponding delay times, and we use all of them in each time bin. Thus, for each bin we have a total of $n_{\text{short}} = 7.6 \times 10^3$ and $n_{\text{long}} = 225 \times 10^3$ progenitors for short and long GRBs, respectively. Each progenitor in our list now represents a fraction of the total SFR density in the given bin that generates GRBs. This fraction is given by

$$f_{\text{sim}} = \frac{F_{\text{pop,II}}}{M_{\text{sim}}} \text{sfr}(t), \qquad (12)$$

where M_{sim} is the total stellar mass corresponding to our population synthesis simulations (see Section 3), and f_{sim} has units of yr^{-1} Gpc^{-3}.

For each progenitor in the list we choose a random starting time, t_0, within the given time bin, and propagate the progenitor formation rate density, f_{sim}, forward in time to

$$t_{\text{new}} = t_0 + t_{\text{del}}. \qquad (13)$$

The delay time, t_{del}, marks the time elapsed from the formation of the star to the potential GRB event, as described in Section 3, and t_{new} is the time at which a given GRB event actually occurs. We thus convert the formation rate density of progenitors into GRB event rate densities. By repeating the above series of steps for each time bin, we arrive at a total comoving GRB event rate density, $n_{\text{rest}}(t)$.

5. INTRINSIC RATES

In this section, we calculate the intrinsic rate of short and long GRBs from Population II progenitors. In the first subsection, we discuss correction factors due to model uncertainties, while in the second subsection, we provide estimates of the intrinsic GRB rates.

5.1. Correction Factors: Population Synthesis

Both the DBH formation and double compact object merger rates obtained from population synthesis are only first-order approximations for long and short duration GRBs, respectively. For example, the only constraints placed on our long-duration GRB progenitors were the assumption that the black hole formed from direct collapse and that the star, at collapse, was a He star.

Observations of nearby GRB/SN associations suggest that the progenitor must lose most of its helium, because, to date, every SN observed associated with a GRB is a type Ic SN (see Fryer et al. 2007 for a recent review). We have not placed additional constraints requiring the loss of the He envelope. In addition, we have not placed constraints on the angular momentum profile, which is likely to play an important role in GRB formation.

The type Ic constraint poses a problem for many of the current progenitor scenarios and, hence, makes it difficult to predict a reliable rate from population synthesis studies alone. Ignoring this constraint, we can make only rudimentary estimates of the GRB event rates. With the rotation rates suggested by Yoon et al. (2006), roughly 10% of the collapsing stars in our simulations form GRBs. Given our rate estimates for both long and short bursts, this indicates that the odds are roughly 10 to 1 that GRB 080913 and 090423 were long-duration bursts. However, Podsiadlowski et al. (2004) have argued that only 1% of all black hole systems would form GRBs. Although these authors mention that this fraction could potentially increase at low metallicity, if we keep their 1% figure we find a long-duration GRB rate 100 times smaller than the one we calculated for the DBH formation channel. Thus, the likely rate for long-duration GRBs is reduced by a factor of $\epsilon_{\rm syn,long} \sim 0.01$–$0.1$.

Our rate for short GRBs is also an overestimate. We include all BH–NS mergers, while neglecting system configuration (inclination/mass ratio) and black hole spin (only 1%–40% of mergers are expected to form BH torus configurations and thus potentially result in a GRB: Belczynski et al. 2008c). If GRBs indeed require the formation of a black hole (e.g., Janka & Ruffert 1996; Oechslin & Janka 2006; Lee & Ramirez-Ruiz 2007), the fraction of NS–NS mergers is limited by the maximum neutron star mass. Most known NS–NS mergers will form central compact objects with masses $M_c \lesssim 2.5\,M_\odot$ (Belczynski et al. 2008b). The maximum neutron star mass must be less than this value, or these mergers will not form black hole accretion disks. However, the requirement of a black hole is a weak constraint as neutron star accretion disks as well as protomagnetars may also produce short GRBs (Usov 1992; Kluzniak & Ruderman 1998; Dai et al. 2006; Metzger et al. 2008). The low-metallicity population of double compact objects consists of ~60% of NS–NS binaries and ~40% of BH–NS systems (see Section 3). Thus the reduction due to the required configuration of BH–NS systems does not lead to a significant decrease of short GRB rates. The likely rate for short-duration GRBs is thus reduced by approximately $\epsilon_{\rm syn,short} \sim 0.6$–$0.8$.

Additionally, the formation rates of double compact objects as calculated in population synthesis are subject to uncertainties that are associated with some poorly understood evolutionary processes that are important in the evolution of massive binaries (e.g., winds, mass transfer episodes, natal kicks). Belczynski et al. (2002) presented a comprehensive parameter study of double compact object formation rates. If the most unrealistic and unphysical models are omitted, it was shown that NS–NS and BH–NS merger rates vary at most by factor of ~6 (up and down) from the reference model (best guess for evolutionary parameters) value. We use this as an estimate of the population synthesis uncertainty in the rates and thus renormalize correction factors to $\epsilon_{\rm syn,short} \sim 0.1$–$4.8$.

In summary, the population synthesis or model-related correction factors are

$$\epsilon_{\rm syn,long} = 0.01\text{–}0.1 \qquad (14)$$

$$\epsilon_{\rm syn,short} = 0.1\text{–}4.8. \qquad (15)$$

5.2. Intrinsic Rate Estimate

Our estimate of the intrinsic GRB event rate density in the rest frame is given by

$$\mathcal{N}_{\rm rest}(t) = \epsilon_{\rm syn}\, n_{\rm rest}(t)\ {\rm yr}^{-1}\,{\rm Gpc}^{-3}, \qquad (16)$$

where $\epsilon_{\rm syn}$ was introduced in the previous subsection, and $n_{\rm rest}$ was introduced in Section 4. The rate density of GRBs that would be observed is appropriately time dilated: $\mathcal{N}_{\rm obs}(t) = \mathcal{N}_{\rm rest}(t)/(1 + z(t))$. In a slightly confusing accident of notation, the units of both of these quantities is ${\rm yr}^{-1}\,{\rm Gpc}^{-3}$, where in one case years are measured in the rest frame of the GRB population, and in the other case years are measured by a clock at the local observatory.

It is to be noted that some events have such long delay times, or are associated with such recent star formation, that the GRB events will happen in our future ($t_{\rm new} > 13.47$ Gyr), and thus are not included in the event rate density estimates. We note that this affects only short GRB progenitors, as delay times for long GRB progenitors are very short (see Figure 2).

We are also interested in the intrinsic GRB event rate, in addition to the event rate density. We present intrinsic event rates in the observer frame. To determine the rate to some specified redshift, z, we integrate the GRB event rate density (modified by time dilation) over the comoving volume:

$$N(<z) = 4\pi \epsilon_{\rm syn} \int_0^z \frac{n_{\rm rest}}{1 + z'} \frac{dV}{dz'} dz'\ {\rm yr}^{-1}, \qquad (17)$$

where we have integrated over the entire sky ($\int d\Omega = 4\pi$). It is important to note that, although the above integral is in redshift, it is integrating out the volume (given by Equation (9)) and not the time; the original units of rate density (${\rm yr}^{-1}\,{\rm Gpc}^{-3}$) have been converted into a rate (${\rm yr}^{-1}$) and not into a density (${\rm Gpc}^{-3}$). $N(<z)$ represents the rate in the observer frame of all GRB events (bursts per year) integrating to a limiting redshift of z. Since N denotes the intrinsic rate, we have not yet applied observational selection effects due to such things as beaming, brightness, or instrumental response (these are calculated in Section 6.1).

The population synthesis code naturally distinguishes between long and short GRBs, and we carry this identification through our calculations, quoting results for both long ($N_{\rm long}$) and short ($N_{\rm short}$) GRBs. The resulting intrinsic GRB rate densities and event rates are shown in Figures 3–5. As expected for long GRBs, these rates closely track the star formation history of Population II stars: the majority (90%) of events are found at redshifts $z \sim 3$–15 with a peak at $z \sim 7$ (fast metallicity evolution model), or at $z \sim 2$–11 with a peak at $z \sim 3$ (slow model). Short Population II GRBs start appearing slightly later than long Population II GRBs, and their distribution extends to lower redshift ($z \sim 0$). However, the peak of the short GRB rate is near the long burst peak, at $z \sim 7$ (fast) and $z \sim 3$ (slow), due to the large abundance of very short delays. We note that even a delay as short as 0.1 Gyr is sufficient to result in many kpc distances between the site of star formation in the host galaxy and the eventual merger location in the halo (e.g., Fryer et al. 1999; Bloom et al. 1999; Belczynski et al. 2006). The short GRB progenitors considered here (NS–NS/BH–NS mergers) have a tail of very long delay times (median 0.1 Gyr and standard deviation
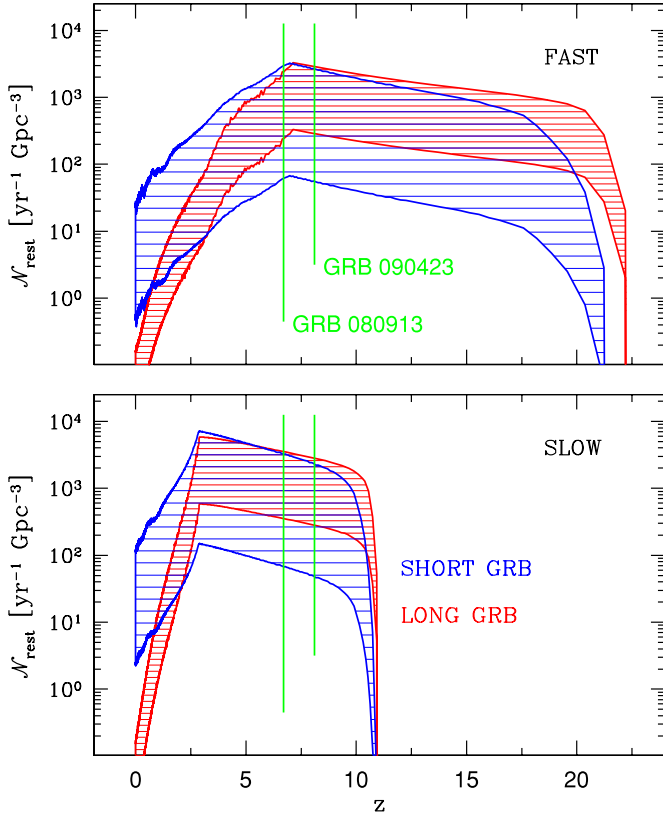
Figure 3. Short and long GRB intrinsic event rate densities (in the rest frame) originating from Population II stars for slow and fast metallicity evolution. These are expressed per year, per cubic comoving Gpc.

(A color version of this figure is available in the online journal.)

Figure 4. Intrinsic event rate of short and long GRBs that originate from Population II stars, per year (in the observer frame), as a function of the depth of the survey in redshift, z. The rates are shown for slow and fast metallicity evolution models.

(A color version of this figure is available in the online journal.)

2.9 Gyr), resulting in substantial intrinsic rates of Population II mergers at low redshift.

We note that in the redshift range $6 < z < 8$, the intrinsic rates for long and short GRBs are comparable (see Figure 5). At redshift $z = 6.7$, the rates are $N_{\rm long} = 10 \times 10^3$–$153 \times 10^3$ yr^{-1} and $N_{\rm short} = 3 \times 10^3$–$141 \times 10^3$ yr^{-1} per unit redshift, in the observer frame. At redshift $z = 8.1$, these rates become $N_{\rm long} = 9 \times 10^3$–$91 \times 10^3$ yr^{-1} and $N_{\rm short} = 2 \times 10^3$–$84 \times 10^3$ yr^{-1} (the ranges encompass both of our metallicity evolution models). The above similarity of rates arises for two reasons: first, the population synthesis rates of short ($\epsilon_{\rm syn,short} n_{\rm short} = 0.8 \times 10^3$–$36.5 \times 10^3$) and long ($\epsilon_{\rm syn,long} n_{\rm long} = 2.3 \times 10^3$–$22.5 \times 10^3$) GRB progenitors are comparable; second, Population II SFRs for the two metallicity evolution models are almost the same ($\sim 0.1\ M_\odot$ yr^{-1} Mpc^{-3}; see Figure 1) at these redshifts.

For comparison, we have also calculated the rate of SNe utilizing the same procedure presented above. The cumulative rate of core collapse SNe (type II and Ib/c) is estimated to be ~ 8 s^{-1} (integrated to redshift $z = 10$), which is comparable to the rates from recent empirical estimates of SFR(z), e.g., Hopkins & Beacom (2006).

6. OBSERVED RATES

In this section, we predict the *Swift* detection rate of short and long GRBs from Population II progenitors. In the first subsection, we discuss observational selection effects, while in the second subsection we provide estimates of the observed GRB rates.
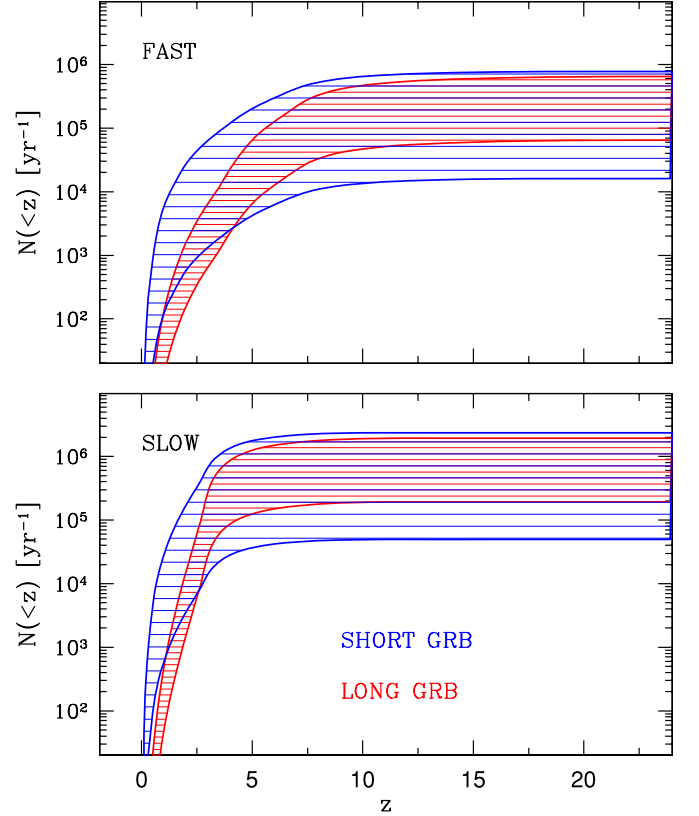
6.1. Correction Factors: Observational Selection Effects

Not all high-redshift GRBs will necessarily be observable. There are many factors which impact whether or not a given GRB will be observed, including the light curve and spectral energy distribution (SED) of the burst (both of them redshifted), as well as the spectral and time sensitivity of the detector. A precise calculation of the selection function of GRBs is well beyond the scope of this paper. The GRB population is tremendously heterogeneous, and the triggering algorithms of an instrument such as the Burst Alert Telescope (BAT) on *Swift* are highly complex (Band 2003, 2006; Fenimore et al. 2004). In what follows we make a number of simplifications, and derive an approximation for the observed rate of short and long GRBs.

We assume that *all* GRBs have the same distribution of average isotropic luminosity, $L_{\rm iso}$, given by a Gaussian in $\log(L_{\rm iso})$, centered on $L_{\rm iso} = 10^{50}$ erg s^{-1}, with $1\sigma = 1$ dex. We assume all short GRBs have a duration of $t_{90} = 0.3$ s, while all long GRBs last $t_{90} = 30$ s. The distributions of total energy (integrated flux; calculated as $\mathcal{E} = L_{\rm iso} t_{90}$) for short and long bursts are presented in Figure 6.

We approximate the *Swift* GRB trigger (for the BAT instrument) as a fluence[7] threshold. We take the long GRB trigger as $\bar{\mathcal{E}}_{\rm long} = 3 \times 10^{50}$ erg for a long burst at $z = 1$ (see, e.g.,

---

[7] Our fluence threshold can easily be rephrased as a trigger on peak flux/luminosity, with all of the units being converted from (erg) to (erg s^{-1}). The results are identical. In addition, we are calculating the fluence from an isotropic luminosity, but the results are unchanged if this is taken to be a beamed luminosity.
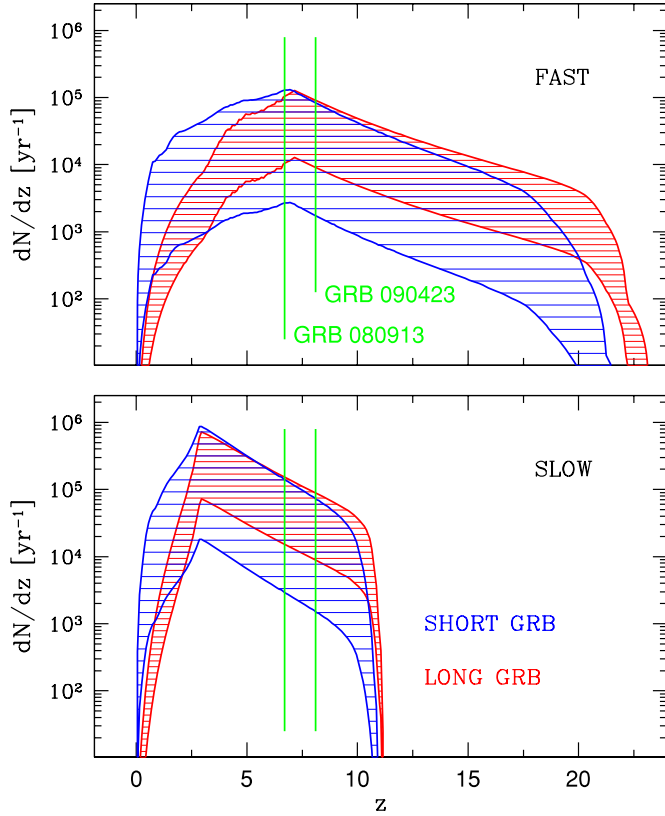
Figure 5. Intrinsic event rate of short and long GRBs that originate from Population II stars, per year (in the observer frame) presented per unit redshift. These plots show the derivative of curves presented in Figure 4, highlighting the redshift range in which GRB events from Population II stars contribute.

(A color version of this figure is available in the online journal.)

Figure 2 of Kistler et al. 2008 and Figure 2 of Butler et al. 2007). In other words, a long GRB at $z = 1$ must emit a total isotropic-equivalent energy satisfying $\mathcal{E} \geqslant 3 \times 10^{50}$ erg to be observable. The corresponding short GRB threshold is given by $\bar{\mathcal{E}}_{\mathrm{short}} = 10^{50}$ erg at $z = 1$. The difference between the thresholds is chosen to mimic some of the complexity in the BAT triggers, including integration and readout times, as well as sensitivity to the differing SEDs of long and short bursts (Fenimore et al. 2004; Band 2003, 2006). For a burst at redshift z, we draw an energy from the relevant distribution shown in Figure 6, and then calculate whether the fluence of the burst satisfies our trigger threshold criterion:

$$\mathcal{E} \geqslant (D_L(z)/D_L(z=1))^2 \, \bar{\mathcal{E}}, \qquad (18)$$

where $D_L(z)$ is the luminosity distance out to redshift z. Only those bursts which satisfy this inequality are taken to be observed. The resulting fraction of long and short bursts observed with *Swift*, ϵ_{SED}, as a function of redshift, is plotted in Figure 6.

Another factor we have not yet considered is beaming, and the resulting visibility of GRBs. In general, short GRB jets appear to be wider, with opening angles of $\Theta \gtrsim 10°$ (e.g., Fox et al. 2005; Berger 2007; Metzger et al. 2009) as compared with long GRBs, $\Theta \sim 5°$ (e.g., Frail et al. 2001; Bloom et al. 2003; Grupe et al. 2006; Soderberg et al. 2006). This would imply that long GRBs are ~4 times less likely to be detected, leading to further reduction of the observed rates by factors of

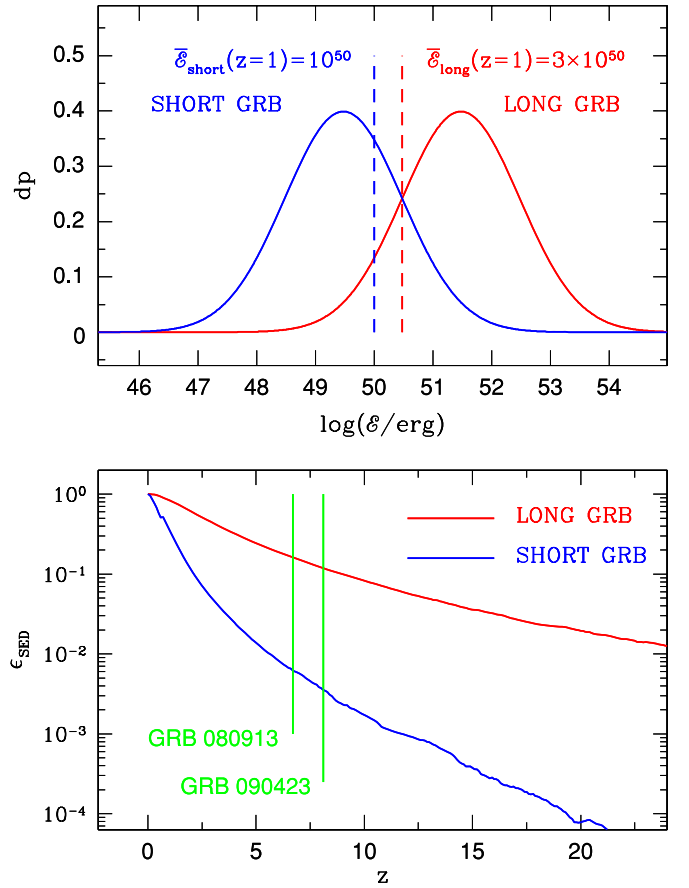$$\epsilon_{\mathrm{beam,long}} = 0.002 \qquad (19)$$

Figure 6. Top panel: distribution of total energy ($\mathcal{E} = L_{\mathrm{iso}}t_{90}$) for short and long GRBs. Short and long GRBs are assumed to have the same distribution of average isotropic luminosity, L_{iso}, described by a Gaussian in $\log(L_{\mathrm{iso}})$ with mean at $\log(L_{\mathrm{iso}}/(\mathrm{erg\ s}^{-1})) = 50$ and $\sigma = 1.0$. A single typical duration time was assumed for all short ($t_{90} = 0.3$ s) and long ($t_{90} = 30$ s) GRBs. The adopted *Swift* detection thresholds (at $z = 1.0$) are also shown; $\bar{\mathcal{E}} = 10^{50}$, 3×10^{50} erg for short and long GRBs, respectively; see the text for details. Bottom panel: the fraction of GRBs above the *Swift* detection limit, ϵ_{SED}, as a function of redshift. Note that at redshift $z = 6.7$ (GRB 080913) the fraction of detectable long GRBs is $\epsilon_{\mathrm{SED,long}} = 0.162$, while for short events it is only $\epsilon_{\mathrm{SED,short}} = 0.006$. At redshift $z = 8.1$ (GRB 090423), the difference in detection probability is even larger: $\epsilon_{\mathrm{SED,long}} = 0.118$ and $\epsilon_{\mathrm{SED,short}} = 0.004$.

(A color version of this figure is available in the online journal.)

$$\epsilon_{\mathrm{beam,short}} = 0.008, \qquad (20)$$

for long and short GRBs, respectively.

6.2. Observed Rate Estimate

We now provide a prediction for the *Swift* detection rate for Population II GRBs. We express rates per unit redshift to emphasize the redshift range relevant for GRB 080913 and GRB 090423. The predicted detection rate is given by

$$\frac{dN_{Swift}}{dz} = f_{Swift}\, \epsilon_{\mathrm{SED}}\, \epsilon_{\mathrm{beam}}\, \frac{dN}{dz}\ \mathrm{yr}^{-1}, \qquad (21)$$

where N is the intrinsic rate of GRBs (see Section 5.2), ϵ_{beam} is a correction factor for GRB beaming (see Section 6.1), ϵ_{SED} is the fraction of GRBs above the *Swift* detection threshold (see Figure 6 and Section 6.1), and $f_{Swift} = 1.4/(4\pi) = 0.1$ represents the *Swift* sky coverage (Gehrels et al. 2004; Barthelmy et al. 2005). We plot our prediction for the observed rate of both short and long GRBs in *Swift* in Figure 7. In the
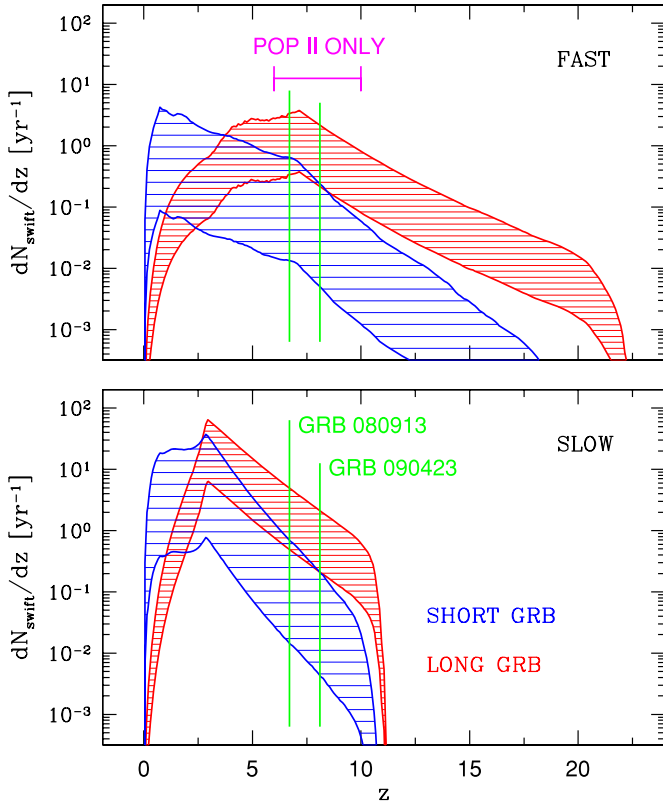
Figure 7. Predicted *Swift* detection rates of short (NS–NS/BH–NS mergers) and long (collapsars) GRBs. Rates are for GRBs originating exclusively from Population II stars, and hence can only be compared to *Swift* data in the redshift range in which Population II stars are the dominant stellar population: $6 \lesssim z \lesssim 10$ (as marked on the plot). For low redshifts ($z \lesssim 6$), there is a significant contribution to GRB rates from Population I stars (not shown here), and for very high redshifts ($z \gtrsim 10$) there may be a contribution from GRBs originating from Population III stars (not shown here). Note that GRB 080913 and GRB 090423 are both found in the redshift range in which the majority of GRB events are predicted to originate from Population II stars. Furthermore, our results favor the collapsar origin for these GRBs. The two panels show the rates for a fast (early metal mixing into stars; top panel) and a slow (late mixing; bottom panel) metallicity evolution model. In the redshift range of interest ($6 \lesssim z \lesssim 10$), the rates of the two extreme models are similar, indicating that our conclusions are robust: GRB 080913 and GRB 090423 have Population II progenitors, and are both long bursts resulting from collapsars.

(A color version of this figure is available in the online journal.)

redshift range $z = 6.2$–7.2 centered on $z = 6.7$ (GRB 080913), we expect *Swift* GRB detection rates of

$$N_{Swift,long} \sim 0.33\text{–}5.0 \text{ yr}^{-1} \quad \text{at } z = 6.2\text{–}7.2 \qquad (22)$$

$$N_{Swift,short} \sim 0.01\text{–}0.70 \text{ yr}^{-1} \quad \text{at } z = 6.2\text{–}7.2. \qquad (23)$$

For the redshift range $z = 7.6$–8.6 centered on $z = 8.1$ (GRB 090423), the predicted *Swift* detection rates become

$$N_{Swift,long} \sim 0.21\text{–}2.2 \text{ yr}^{-1} \quad \text{at } z = 7.6\text{–}8.6 \qquad (24)$$

$$N_{Swift,short} \sim 0.004\text{–}0.24 \text{ yr}^{-1} \quad \text{at } z = 7.6\text{–}8.6. \qquad (25)$$

These results suggest that GRB 080913 and GRB 090423 are most likely associated with the deaths of massive stars (long GRBs), rather than double compact object mergers (short GRBs). At redshifts $z = 6.7$ (GRB 080913) and $z = 8.1$ (GRB 090423) long GRBs are expected to be $\sim$10 times more frequent than short GRBs in the *Swift* sample. We emphasize

that we have taken an optimistic value for the short burst observational threshold; the true short GRB rate may be up to an order of magnitude smaller (see Section 6.1 for details). Our results thus represent an upper limit to the short GRB fraction at these high redshifts. Although the intrinsic event rates for collapsars and double compact object mergers are similar at these high redshifts, the observational difference is due to the very distinct observational selection effects between these two event types. We note that our results are consistent with Zhang et al. (2009), who classified both bursts as collapsars based upon their observational properties. We have ignored recent evidence that the long GRB population evolves with redshift, increasing the number of observed bursts at high redshift. In this sense, our results can be considered a lower limit to the long GRB rate (although we note that the corresponding evolution of short bursts is currently poorly constrained). Further details of the nature of GRB intrinsic properties and observational selection effects can be found, for example, in Guetta et al. (2005), Guetta & Piran (2006), Berger (2007), Kistler et al. (2008), Salvaterra et al. (2009), and Virgili et al. (2009).

7. SUMMARY

We have calculated the evolution of stars at high redshift, exploring possible progenitors for GRB 080913 (at $z = 6.7$) and GRB 090423 (at $z = 8.1$). We find that in the redshift range $6 \lesssim z \lesssim 10$ the majority of stars are Population II (low metallicity). By this time, Population III stars (metal free) have already finished their evolution, and Population I stars (metal rich) are only just beginning to form. We have adopted two extreme models for the metallicity evolution history, which most likely bracket the true history; our final results are insensitive to the choice of model. We find that the progenitors of GRB 080913 and GRB 090423 are likely to have been Population II stars.

For Population II stars we subsequently calculated the rates of double compact object mergers (NS–NS and BH–NS) and the rates of collapsars (deaths of massive stars). The former are thought to be associated with short GRBs, while the latter are believed to be responsible for long GRBs. We find that the intrinsic rates for short GRBs (mergers) and long GRBs (collapsars) are comparable at high redshift (see Figure 5). However, the observational selection effects (beaming, differing intrinsic fluence, and instrumental response) make long bursts more likely to be seen by a satellite like *Swift*. Our main result is shown in Figure 7, where we plot our predicted *Swift* detection rates for both short and long GRBs. On average, the detection rates for long GRBs are 10 times higher than the rates for short GRBs. At the redshifts of GRB 080913 and GRB 090423, the rates are $\sim$1 yr^{-1} and $\sim$0.1 yr^{-1} per unit redshift, for long and short GRBs, respectively. We emphasize that our calculations only consider Population II stars, as these stars dominate the SFR at redshift $6 \lesssim z \lesssim 10$ (see Figure 1), and are thus appropriate for the two highest known redshift GRBs. In future work, we will include all generations of stars.

We conclude that both GRB 080913 and GRB 090423 are most likely to have been long bursts, resulting from the deaths of massive stars (collapsars) from Population II progenitors. With the observation of GRB 080913 and 090423, GRBs have entered a unique high-redshift regime. As future data fill out the high-z tail of GRBs, these systems will become one of the most powerful probes of the star formation, stellar death, and chemical enrichment of our universe.

REFERENCES

Abt, H. A. 1983, ARA&A, 21, 343
Amati, L. 2006, MNRAS, 372, 233
Band, D. L. 2003, ApJ, 588, 945
Band, D. L. 2006, ApJ, 644, 378
Barthelmy, S. D., et al. 2005, Space Sci. Rev., 120, 143
Beers, T., & Christlieb, N. 2005, ARA&A, 43, 531
Belczynski, K., Bulik, T., Heger, A., & Fryer, C. L. 2007, ApJ, 664, 986
Belczynski, K., Kalogera, V., & Bulik, T. 2002, ApJ, 572, 407
Belczynski, K., Kalogera, V., Rasio, F., Taam, R., Zezas, A., Bulik, T., Maccarone, T., & Ivanova, N. 2008a, ApJS, 174, 223
Belczynski, K., O'Shaughnessy, R., Kalogera, V., Rasio, F., Taam, R. E., & Bulik, T. 2008b, ApJ, 680, L129
Belczynski, K., Perna, R., Bulik, T., Kalogera, V., Ivanova, N., & Lamb, D. 2006, ApJ, 648, 1110
Belczynski, K., Taam, R. E., Rantsiou, E., & van der Sluys, M. 2008c, ApJ, 682, 474
Berger, E. 2007, ApJ, 670, 1254
Binney, J., & Merrifield, M. 1998, Galactic Astronomy (Princeton, NJ: Princeton Univ. Press)
Bloom, J. S., Butler, N. R., & Perley, D. A. 2008, in AIP Conf. Proc. 1000, Gamma-Ray Bursts 2007, ed. M. Galassi, D. Palmer, & E. Fenimore (Melville, NY: AIP), 11
Bloom, J. S., Frail, D., & Kulkarni, S. 2003, ApJ, 594, 674
Bloom, J. S., Sigurdsson, S., & Pols, O. 1999, MNRAS, 305, 763
Butler, N. R., et al. 2007, ApJ, 671, 656
Cheng, K., & Dai, Z. 1996, Phys. Rev. Lett., 77, 1210
Clark, J., Muno, M., Negueruela, I., Dougherty, P., Crowther, P., Goodwin, S., & de Grijs, R. 2008, A&A, 477, 147
Cusumano, G., et al. 2006, Nature, 440, 164
Dai, Z., Wang, X., Wu, X., & Zhang, B. 2006, Science, 311, 1127
Dar, A., & Rujula, A. 2004, Phys. Rep., 405, 203
Donaghy, T. Q., et al. 2006, arXiv:astro-ph/0605570
Duquennoy, A., & Mayor, M. 1991, A&A, 248, 485
Eichler, D., Livio, M., Piran, T., & Schramm, D. 1989, Nature, 340, 126
Erb, D., et al. 2006, ApJ, 644, 813
Fenimore, E., et al. 2004, Baltic Astron., 13, 301
Fontana, A., et al. 2006, A&A, 459, 745
Fox, D., et al. 2005, Nature, 437, 845
Frail, D., et al. 2001, ApJ, 562, L55
Fryer, C. L., & Kalogera, V. 2001, ApJ, 554, 548
Fryer, C. L., Woosley, S., & Hartmann, D. H. 1999, ApJ, 526, 152
Fryer, C. L., et al. 2007, PASP, 119, 1211
Galama, T., et al. 1998, Nature, 395, 670
Gehrels, N., et al. 2004, ApJ, 611, 1005
Gou, L., et al. 2004, ApJ, 604, 508
Greiner, J., et al. 2009, ApJ, 693, 1610
Grindlay, J. 2006, in AIP Conf. Proc., Vol. 836, Gamma-ray Bursts in the Swift Era, ed. S. S. Holt, N. Gehrels, & J. A. Nousek (Melville, NY: AIP), 631
Grupe, D., et al. 2006, ApJ, 653, 462
Guetta, G., & Piran, T. 2006, A&A, 453, 823
Guetta, G., Piran, T., & Waxman, E. 2005, ApJ, 619, 412
Hartmann, D. H. 2008, New Astron. Rev., 52, 450
Hartmann, D. H., et al. 2009, "Tracing the Cosmic Star Formation History to its Beginnings: GRBs as Tools," Astro2010 White Paper, no. 115
Heger, A., Fryer, C. L., Woosley, S. E., Langer, N., & Hartmann, D. H. 2003, ApJ, 591, 288

Heggie, D. C. 1975, MNRAS, 173, 729
Hjorth, J., et al. 2003, Nature, 423, 847
Hogg, D. W. 2000, arXiv:astro-ph/99055116
Hopkins, A., & Beacom, J. 2006, ApJ, 651, 142
Hurley, J., Pols, O., & Tout, C. 2000, MNRAS, 315, 543
Iye, M., et al. 2006, Nature, 443, 186
Janka, H.-T., & Ruffert, M. 1996, A&A, 307, L33
Kawai, N., et al. 2006, Nature, 440, 184
King, A., Olsson, E., & Davies, M. 2007, MNRAS, 374, L34
Kistler, M., Yuksel, H., Beacom, J., & Stanek, K. 2008, ApJ, 673, L119
Kluzniak, W., & Ruderman, M. 1998, ApJ, 505, L113
Kroupa, P., Tout, C. A., & Gilmore, G. 1993, MNRAS, 262, 545
Kroupa, P., & Weidner, C. 2003, ApJ, 598, 1076
Lamb, D. Q. 2007, Phil. Trans. R. Soc. A:, 365, 1363
Lamb, D. Q., & Reichart, D. 2000, ApJ, 536, 1
Lee, W. H., & Ramirez-Ruiz, E. 2007, New J. Phys., 9, 17
Lloyd-Ronning, N. M., Fryer, C. L., & Ramirez-Ruiz, E. 2002, ApJ, 574, 554
MacFadyen, A. I., & Woosley, S. E. 1999, ApJ, 524, 262
Mackey, J., Bromm, V., & Hernquist, L. 2003, ApJ, 586, 1
Metzger, B., Piro, A., & Quataert, E. 2009, MNRAS, 396, 304
Metzger, B., Quataert, E., & Thompson, T. 2008, MNRAS, 385, 1455
Nakar, E. 2007, Phys. Rep., 442, 166
Oechslin, R., & Janka, H.-T. 2006, MNRAS, 368, 1489
O'Shea, B. W., & Norman, M. L. 2007, ApJ, 654, 660
Paczynski, B. 1986, ApJ, 308, L43
Pei, Y., Fall, M., & Hauser, M. 1999, ApJ, 522, 604
Perez-Ramirez, D., et al. 2008, A&A, submitted (arXiv:0810.2107)
Piro, L., et al. 2009, Exp. Astron., 23, 67
Podsiadlowski, Ph., Mazzali, P. A., Nomoto, K., Lazzati, D., & Cappellaro, E. 2004, ApJ, 607, L17
Popham, R., Woosley, S. E., & Fryer, C. L. 1999, ApJ, 518, 356
Prochaska, J. X., Chen, H.-W., Dessauge-Zavadsky, M., & Bloom, J. S. 2007, ApJ, 666, 267
Ripamonti, E., & Abel, T. 2004, MNRAS, 348, 1019
Ruffini, R., et al. 2006, ApJ, 645, 109
Salvaterra, R., Guidorzi, C., Campana, S., Chincarini, G., & Tagliaferri, G. 2009, MNRAS, 396, 299
Salvaterra, R., et al. 2009, Nature, 461, 1258
Sana, H., Gosset, E., Naze, Y., Rauw, G., & Linder, N. 2008, MNRAS, 386, 447
Savaglio, S., Glazebrook, K., & LeBorgne, D. 2009, ApJ, 691, 182
Schaerer, D. 2002, A&A, 382, 28
Schady, P., et al. 2008, GCN Circular., 8217, 1
Schneider, R., Salvaterra, R., Ferrara, A., & Ciardi, B. 2006, MNRAS, 369, 825
Smith, B., et al. 2009, ApJ, 691, 441
Soderberg, A., et al. 2006, ApJ, 650, 261
Stamatikos, M., et al. 2008, GCN Circular., 8222, 1
Stanek, K., et al. 2003, ApJ, 591, L17
Strolger, L., et al. 2004, ApJ, 613, 200
Tanvir, N. R., et al. 2009, Nature, 461, 1254
Tornatore, L., Ferrara, A., & Schneider, R. 2007, MNRAS, 382, 945
Tremonti, C., et al. 2004, ApJ, 613, 898
Usov, V. 1992, Nature, 357, 472
Virgili, F., Liang, E., & Zhang, B. 2009, MNRAS, 392, 91
Vreeswijk, P., et al. 2008, GCN Circular, 8221, 1
Willot, C., et al. 2007, AJ, 134, 2435
Woosley, S. 1993, ApJ, 405, 273
Woosley, S., & Bloom, J. 2006, ARA&A, 44, 507
Yoon, S.-C., Langer, N., & Norman, C. 2006, A&A, 460, 199
Young, P., & Fryer, C. L. 2007, ApJ, 670, 584
Zhang, B., Zhang, B.-B., Liang, Gehrels, N., E.-W., Burrows, D. N., & Mészáros, P. 2007, ApJ, 655, L25
Zhang, B., et al. 2009, ApJ, 703, 1696